ARTICLE OPEN

Check for updates

# CLN5 deficiency impairs glucose uptake and uncovers PHGDH as a potential biomarker in Batten disease

Maria Marchese[1]✉, Sara Bernardi[1], Rachele Vivarelli[1], Stefano Doccini[1], Lorenzo Santucci[1], Asahi Ogi[1], Rosario Licitra[2], Jingjing Zang[3], Rabah Soliymani[4], Serena Mero[1], Stephan CF Neuhauss[3], Lea Ciarmoli[5], Giovanni Signore[5,6], Maciej M. Lalowski[4,7] and Filippo M. Santorelli[1]✉

© The Author(s) 2025

CLN5 disease, a form of juvenile dementia within the neuronal ceroid lipofuscinosis (NCL), is associated with mutations in the *CLN5* gene encoding the lysosomal bis(monoacylglycero)phosphate (BMP) synthase, essential for BMP production and lysosomal function. Limited knowledge of cellular mechanisms and unclear drug targets hinder translating this to children's treatment, which remains symptomatic. We developed and characterized a new *cln5* knock-out zebrafish model that replicates key features and molecular signatures of the human disease. Loss of Cln5 function in vivo altered axonal growth of retinal ON-bipolar cells and disrupted calcium homeostasis in the cerebellum, revealing new disease features. Additionally, multi-omic analyses at different developmental stages revealed an impaired glucose metabolism as an original finding in NCL. A novel biomarker, PHGDH, was validated in zebrafish and human skin fibroblasts harboring pathogenic variants in *CLN5*, and in *CLN7*. We also tested metformin which improved the expression of PHGDH in patient-derived cells, and rescued zebrafish behavior. This work demonstrates the profound metabolic impact of CLN5 dysfunction, offering a promising avenue toward targeted therapies for juvenile dementia.

*Molecular Psychiatry*; https://doi.org/10.1038/s41380-025-03043-8

## INTRODUCTION

The neuronal ceroid-lipofuscinoses (NCLs), also known as Batten disease, are neurometabolic lysosomal storage disorders and collectively represent the most frequent childhood-onset neurodegenerative diseases and the main cause of childhood dementia in Europe [1]. NCLs are characterized clinically by the combination of myoclonus, seizures, blindness, and progressive neurodegeneration leading to dementia. Lacking in most cases specific therapies [2, 3], both life expectancy and quality of life are limited in NCL children. The CLN5 disease (MIM: 256731) represents an ultra-rare variant late-infantile form of NCL with onset between 4 and 7 years, caused by biallelic mutations in *CLN5*. CLN5 is highly expressed in the cerebellar Purkinje cells (PCs), cortical neurons and hippocampal pyramidal cells, and hippocampal interneurons [4], all areas known to be degenerated in CLN5 human brains [5]. Importantly, hypomorphic gene variants in *CLN5* also occur in other relatively more common genetic conditions such as autosomal recessive macular dystrophy [6], or cerebellar ataxia [7], or even in common neurodegenerative disorders with impaired vision, cognition, and movement disorders, including Alzheimer's Disease (AD) and Parkinson's Disease (PD) [8–10]. This implies that research data gathered in the ultra-rare CLN5 can serve to decipher multiple disease conditions. A recent outbreak in the field demonstrated that *CLN5* encodes the lysosomal bis(monoacylglycero)phosphate synthase (BMPS), the enzyme responsible for the production of bis(monoacylglycero)phosphate (BMP; also called lipid lysobisphosphatidic acid, LBPA) [11]. BMPS-deficient cells exhibited a massive accumulation of the BMP synthesis precursor lysophosphatidylglycerol (LPG), depletion of BMP species, and dysfunctional lipid metabolism [11]. BMP is thought to play a role in glycosphingolipid degradation and cholesterol transport, although the precise mechanism of its biosynthesis and transport remains still unclear. In line with the alterations in lipids, the mitochondrial-lysosome interplay, lipid homeostasis, and sphingolipid metabolism we had shown in knock-out SH-SY5Y neuronal-like cells [12], new findings on CLN5 function [11] imply that neuronal cells may be especially susceptible to lysosomal disruptions, a feature already known in early biochemical work from cerebral cortex in NCL patients [13]. Interestingly, alterations of BMP levels have been observed in several human diseases [14, 15], suggesting that pharmacologically activating and inhibiting the BMP synthase can exert therapeutic effects not only in lysosomal storage disorders such as CLN5 but also in more common forms of dementia [16].

In this light, comprehending metabolic alterations caused by CLN5 impairment during development may constitute a burgeoning research area underlying potential treatments for neurodegenerative disorders, such as juvenile-onset neuronal ceroid lipofuscinoses.

Zebrafish represents a valid model to study the pathomechanisms in NCLs [12, 17–20], and for drug discovery [20]. The main

[1]Neurobiology and Molecular Medicine Unit, IRCCS Fondazione Stella Maris, 56128Calambrone, Pisa, Italy. [2]Department of Veterinary Sciences, University of Pisa, 56124 Pisa, Italy. [3]University of Zurich, Department of Molecular Life Sciences, 8057 Zurich, Switzerland. [4]Meilahti Proteomics Unit, Department of Biochemistry & Developmental Biology, Faculty of Medicine, University of Helsinki, 00290 Helsinki, Finland. [5]Department of Biology, University of Pisa, 56126 Pisa, Italy. [6]Institute of Clinical Physiology, National Research Council, 56124 Pisa, Italy. [7]Institute of Molecular Biology and Biotechnology, Faculty of Biology, Adam Mickiewicz University, Uniwersytetu Poznańskiego 6 St., 61-614 Poznań, Poland. ✉email: maria.marchese2086@gmail.com; filippo3364@gmail.com

Received: 11 November 2024 Revised: 14 April 2025 Accepted: 30 April 2025
Published online: 09 May 2025

advantage of zebrafish models resides in tackling complex biological problems and offers insight into the cellular processes that influence disease in relatively simpler organisms with high synteny and sequence identity with human genome.

Herewith, we generated a novel *cln5* knockout zebrafish model. Comprehensive behavioral, physiological and molecular characterization of the *cln5*$^{-/-}$ model highlights its potential for investigating the in vivo mechanisms underlying BMP alteration, and for developing new small-molecule therapies for NCLs.

## MATERIALS AND METHODS

### Zebrafish maintenance

Experiments were conducted on a *cln5*$^{-/-}$ and also on a transgenic [*Tg(neurod1:GCaMP6F)*] line (kindly donated by Claire Wyart of the Institut du Cerveau et de la Moelle Épinière, Paris, France) [21] in the nacre (*mitfa*$^{-/+}$) background, which will henceforth be referred to as wild-type (WT). We used the *mitfa*$^{-/-}$ background for calcium imaging analyses, whereas the *mitfa*$^{-/+}$ fish were used for the other experiments. We had previously verified the absence of any behavioral differences between the [*mitfa*$^{-/+}$*; Tg (neurod1:GCaMP6F)*] line and the standard AB line [22]. Moreover, for the analysis of retinal bipolar ON-cells we used the transgenic line *Tg(nyx:mYFP)* (kindly donated by Jeff S. Mumm of the Wilmer Eye Institute, Johns Hopkins University, Baltimore, MD) [23], while for the analysis of Purkinje cell layer we use the line *Tg(aldoca:GAL4FF)* line [24]. The *cln5*$^{-/-}$ experimental fish were generated by intercrossing *cln5*$^{-/-}$ males and females. Adults were housed in tanks at a density of no more than five zebrafish per liter at a constant temperature of 28.5 °C with a 14-h light/10-h dark cycle. Zebrafish eggs and embryos were collected and grown at 28.5 °C in egg water obtained using "Instant Ocean" sea salts (60 µg/mL) (Aquarium Systems, Sarrebourg, France) and in E3 medium (5 mM NaCl, 0.17 mM KCl, 0.33 mM $CaCl_2$ $2H_2O$, and 0.33 mM MgSO4, per 1 L of deionized water), respectively, according to established procedures [25, 26]. They were staged in either hour post fertilization (hpf) or days post fertilization (dpf). All compounds used for E3 medium solution preparation were purchased from Sigma-Aldrich (St. Louis, MO). The generation of the mutant, using CRISPR/Cas9 technology, was performed with the ethical approval of the Italian Ministry of Health (approval n° 584/2019-PR), in accordance with the European Union's Directive 2010/63/EU on the protection of animals used for scientific purposes, under the supervision of the University of Pisa Animal Care and Use Committee, and in compliance with the 3 R principles. In this study, blinding was not applied during the experimental procedures, as the researchers were aware of the group assignments (wild-type vs. mutant). However, randomization was employed to minimize potential bias in the allocation of experimental units. Additionally, the individuals assessing the outcomes were blinded to the group allocations to prevent bias in evaluating the results. The data analysts were also unaware of the group identities during the analysis, with this information being revealed only after the analysis was completed to ensure objectivity.

### Establishing mutant lines

The selected sgRNA was chosen among the top targets identified by the CHOPCHOP software (www.chochop.rc.fas.harvard.edu/index.php) set with NGG PAM sites and zero predicted off-targets (fewer than three mismatches in the *cln5*-targeting 20-mer). The sgRNA was designed against exon two of the *cln5* transcript (ENSDART00000110866.4) (Supplementary Table S1), and generated as already described [20]. The optimized Cas9 mRNA, for genome editing in zebrafish, was transcribed from a linearized template plasmid pCS2-nCas9n using the mMESSAGE mMACHINE™ SP6 Transcription Kit (Thermo Fisher Scientific, Waltham, MA). The injection strategy has been performed as already described [20].

### Genotyping

For mutation screening, sgRNA-injected F0 embryos, raised to adulthood and outcrossed with the *Tg(neurod1:GCaMP6F)* line, were used to obtain heterozygous F1 embryos. Adults potentially carrying mutations were identified by PCR and fragment analysis using genomic DNA from 10 randomly selected F1 embryos. The sequences of the primers used are listed in Supplementary Table S1. Heterozygous F1 fish carrying a 2-bp deletion and missense mutation in the target site were selected and inter-crossed to generate the homozygous F2 *cln5*$^{-/-}$ line.

### In situ hybridization

Whole-mount in situ hybridization was performed in 5 dpf WT larvae as described elsewhere [27]. The sequences of the primers used can be found in Supplementary Table S1.

### Analysis of larval morphology

Live zebrafish at 5 dpf were mounted on glass depression slides with 1% low melting point agarose. Images were obtained using a Leica M205FA stereomicroscope (Leica Microsystems, Wetzlar, Germany). Zebrafish standard body length, eye size, and yolk sac area were measured using Danioscope software (Noldus Information Technology Wageningen, The Netherlands) [22].

### Quantitative (q)RT-PCR

Gene expression levels of *cln5* mRNA used RNA pooled from WT and *cln5*$^{-/-}$ larvae. Total RNA was extracted from 30 larvae at 120 hpf using the Quick RNA Miniprep Kit (Zymo Research, Irvine, CA) according to the manufacturer's instructions. Extraction of cDNA and qRT-PCR were performed as described elsewhere [27]. Relative expression levels of each gene were calculated using the $2^{-\Delta\Delta CT}$ method [28]. The results obtained in at least three independent experiments were normalized to the expression of the housekeeping gene, *β-actin* (ENSDARG00000037746). The expression analysis of *cln5* mRNA in mutant larvae was calculated setting the mean of the controls at one, and the p-value was calculated using GraphPad Prism 6 software (GraphPad Software Inc., San Diego, CA). The primers used are listed in Supplementary Table S1.

### Mitochondrial respiratory analysis

Mitochondrial respiratory parameters from a mito-stress test were analyzed in control n = 51 (WT) and homozygous *cln5*$^{-/-}$ larvae n = 51 at 120 hpf using the XF24 extracellular flux analyzer (Seahorse Bioscience, North Billerica, MA, USA). The experiment was performed in triplicate. A standard approach was used to measure basal respiration, ATP production, maximal respiration rate, and spare respiratory capacity [22].

### BMP lipid dosage

In order to evaluate the activity of Cln5 we measured in zebrafish the production of the lipid (18:1/18:1) BMP (S,S) by LC-MS analysis. Lipids were extracted from the *cln5*$^{-/-}$ mutant and WT whole brain using a modification of a previously reported method [29]. Briefly, extracted brains were frozen at −80 °C until processed. Next, the sample was put in a 1.5 ml microcentrifuge tube and diluted with 100 µl of 150 mM NaCl aqueous solution and 600 µl of 0.0625 µM DMS (N, N-dimethylsphingosine) in MeOH/$CHCl_3$ 1/2. The biphasic solution was incubated at 25 °C for 30 min at 1000 rpm and then centrifuged at 13.000 rpm for 10 min at 4 °C. The lower chloroform phase was recovered, concentrated *in vacuo*, and reconstituted in a MeOH/H2O/i-PrOH 50/45/5 with 0.1% HCOOH and 1 mM ammonium formate and processed immediately. LC-MS analyses were performed in an Orbitrap Exploris 120 mass spectrometer, interfaced with a Vanquish HPLC chromatograph. Analyses were carried out on a Phenomenex Proteo column (150 × 0.3 mm) at a flow rate of 5 µL/min using MeOH/H2O/i-PrOH 50/45/5 with 0.1% HCOOH and 1 mM ammonium formate (phase A) and MeOH/i-PrOH 50/50 with 0.1% HCOOH and 1 mM ammonium formate (phase B), with the following gradient: 10% B (2 min), 90% B (45 min), 90% B (50 min). Mass analysis was performed with a 150–1000 *m/z* scan at a resolution of 120.000. The area of the peaks of interest was measured and normalized to the signal of DMS (internal standard). Metabolites were harvested in 80% methanol with isotopically labeled amino acids and stored at −80 °C until analysis by LC-MS/MS.

### Western blotting

Larvae collected at 120 hpf (n = 60) in triplicates were lysed in M-PER buffer (Cell Signaling Technology Inc., Danvers, MA) and Western blotting was performed as described elsewhere [20]. The following antibodies were used: anti-LC3 (NB100-2220, Novus Biologicals, Centennial, CO; 1:1000), anti-LAMP1 (ab24170, Abcam, Cambridge, UK, 1:500), anti-β-actin (GTX629630, GeneTex, Irvine, CA; 1:2500), anti-vinculin (ab91459, Abcam, Cambridge, UK, 1:10000) and anti-PHGDH (ORB582487, Biorbyt, Cambridge, UK, 1:100).

## RNA-seq analysis

The whole transcriptomic analysis was carried out on zebrafish 5dpf *cln5*$^{-/-}$ and WT larvae. The WT larvae were also analyzed as a reference (Ctrl). Total RNA was extracted from larvae at 5 dpf ($n = 36$ larvae per group) using the Quick RNA miniprep kit (ZymoResearch, Irvine, CA), according to the manufacturer's instructions, and checked for purity using NanoPhotometerTM Pearl, version 1.2 (IMPLEN, Westlake Village, CA); integrity (RNA integrity number >7) was assessed using the RNA 6000 Pico Kit on a Bioanalyzer 2100 (Agilent Technologies, Santa Clara, CA). Indexed cDNA libraries were prepared from 350 ng of total RNA using the TruSeq Stranded kit (Illumina, San Diego, CA), quantified by real-time PCR, pooled at equimolar concentration, and sequenced with Illumina technology applying standard manufacturer protocols. The quality of reads was assessed using FastQC software Version 0.11.9 (http://www.bioinformatics.babraham.ac.uk/projects/fastqc/). Raw reads with more than 10% of undetermined bases or more than 50 bases with a quality score <7 were discarded. Subsequently, reads were clipped from adapter sequences using Scythe software Version 0.994 (https://github.com/vsbuffalo/scythe), and low-quality ends (Q score <20 on a 15-nt window) were trimmed with Sickle (https://github.com/vsbuffalo/sickle). Filtered reads were aligned to the current zebrafish reference genome assembly (GRCz11) using the STAR aligner (http://code.google.com/p/rna-star).

## Proteomic analysis

*Sample preparation, proteolytic digestion, nano LC-MS/MS and data analysis*. Zebrafish brains, eyes, and whole embryos were separately homogenized by adding a lysis buffer containing 8 M urea (Fisher Chemical, Germany), 0.1 M ammonium bicarbonate (ThermoFisher, Germany), 1% sodium deoxycholate (Thermo scientific, Italy), 0.1% Octyl α- D -glucopyranoside (Fluka, USA), and using Precellys®24 tissue homogenizer (Bertin Technologies, France). Proteins were reduced and alkylated using tris (2-carboxyethyl) phosphine (Aldrich, USA) and iodoacetamide (Sigma-Aldrich, USA) to a final concentration of 5 mM and 50 mM, respectively, and an incubation in the dark for 30 min. Ten micrograms of protein amounts were washed 6 times with 8 M urea, 0.1 M ammonium bicarbonate in Amicon Ultra-0.5 centrifugal filters (Millipore, Merck KGaA, Germany) using a modified FASP method [30, 31]. The peptides were separated by Ultimate 3000 LC system (Dionex, Thermo Scientific) equipped with a reverse-phase trapping column RP-2TM C18 trap column (0.075 x 10 mm, Phenomenex, USA), followed by analytical separation on a bioZen C18 nano column (0.075 × 250 mm, 2.6 µm particles; Phenomenex, USA). The injected sample analytes were trapped at a flow rate of 5 µl x min-1 in 100% of solution A (0.1% formic acid). After trapping, the peptides were separated with a linear gradient of 125 min comprising 110 min from 3 to 35% of solution B (0.1% formic acid/80% acetonitrile), 6 min 45% B, and 4 min to 95% of solution B. Each sample run was followed by at least one empty run to reduce the sample carryover from previous runs. LC-MS acquisition data was done with the mass spectrometer (Thermo Q Exactive HF) settings as follows: The resolution was set to 120,000 for MS scans, and 15000 for the MS/MS scans. Full MS was acquired from 350 to 1400 *m/z*, and the 15 most abundant precursor ions were selected for fragmentation with 45 s dynamic exclusion time. Ions with 2 + , 3 + , 4 + , and 5+ charges were selected for MS/MS analysis. Maximum IT were set as 50 and 80 ms and AGC targets were set to $3e^6$ and $1e^5$ counts for MS and MS/MS respectively. Secondary ions were isolated with a window of 1 *m/z* unit. Dynamic exclusion was set with a duration of 45 s. The NCE collision energy stepped was set to 28 kJ mol–1. Following LC-MS/MS acquisition, raw files were qualitatively analyzed by Proteome Discoverer (PD), version 2.5 (Thermo Scientific, USA). The identification of proteins by PD was performed against the zebrafish protein databases (NCBI and SwissProt, downloaded in June 2023 with 45300 and 3277 entries, respectively) using the built-in SEQUEST HT engine. The following parameters were used: 10 ppm and 0.02 Da were tolerance values set for MS and MS/MS, respectively. Trypsin was used as the digesting enzyme, and two missed cleavages were allowed. The carbamidomethylation of cysteine residues was set as a fixed modification, while the oxidation of methionine, deamidation of asparagine and glutamine, and phosphorylation of serine and threonine were set as variable modifications. The false discovery rate was set to less than 0.01 and a peptide minimum length of six amino acids. Label-free quantification was done using unique peptides in Precursor Ion Quantifier.

*Bioinformatic analysis and categorization of data*. Zebrafish brain and eyes were collected at different developmental stages, including 6 hpf and adult one. Samples were processed, as described elsewhere [32] and used for data dependent acquisition proteome analysis DDA.

The NCBI and Swiss-Prot protein identifiers were further curated by adding the knowledge-based zebrafish IDs (ZFIDs, https://zfin.org/). However, it is important to note that the annotation of the zebrafish proteome remains incomplete, which can limit the identification of certain proteins, particularly less characterized or evolutionary divergent ones. Differentially expressed proteins (DEPs) were identified based on the number of unique peptides used for label-free quantitation (≥2), with an FDR < 0.01 and a fold change (FC) from averaged, normalized protein intensities diverging by >20%, both in up- and in down-regulation, and $p \leq 0.05$ by ANOVA, in *cln5*$^{-/-}$ versus the control group. Bioinformatic analysis was performed using the Ingenuity Pathway Analysis software platform (version: 111725566, release number: summer release, Q2 2024—June 2023; QIAGEN, Hilden, Germany) [33].

To assess gene expression, the normalized expression values for each transcript were calculated as Fragments Per Kilobase per Million mapped reads (FPKM). The expression profile of mutant *cln5*$^{-/-}$ larvae was compared to the profile of WT and for each gene the ratio between average FPKM was calculated and reported as log2 fold change (log2FC). Transcripts showing a FC |≥2| and a False Discovery Rate (FDR, q-value) ≤0.01 were considered to estimate the predicted pathway activation or inhibition, and graphically represented.

To recognize the meaningful biological processes and molecular pathways, we performed a *Core Analysis* using the curated information from the QIAGEN Knowledge Base. The strength of the correlation between a subset of differentially expressed genes / proteins (DEGs/DEP) and a given biological function or disease was expressed by the p-value (calculated using a right-tailed Fisher's Exact Test with Benjamini and Hochberg correction), whereas a "z-score" predicted the activation or inhibition of the given biological context. The macro-categories of Lipid Metabolism and Metabolic Disease were further scrutinized.

## Glucose uptake assay

An adapted Glucose Uptake-Glo™ Assay (Promega, Madison, WI) was performed on 96 hpf zebrafish to assess differences in the rate of glucose uptake between experimental groups, and following the already available protocol [34]. The protocol was adapted using a pool of 10 larvae for each experimental group. Moreover, we performed also an in vivo glucose uptake assay by using 2-deoxy-2-[(7-nitro-2,1,3-benzoxadiazol-4-yl)amino]-D-glucose (2-NBDG; Cayman Chemical Ann Arbor, MI). The larvae at 5dpf were incubated with 2-NBDG (600 µM) in E3 water for 3 h. After incubation, the larvae were rinsed with E3 water, using 0.04% tricaine anesthesia larvae were imaged using a using a Leica M205FA stereo-microscope (Leica Microsystems, Wetzlar, Germany), and fluorescence analysis was quantified using Image J v.1.46, calculating the fluorescent intensity in the region of interest (ROI).

## Live staining imaging

To visualize apoptotic cells, in vivo staining was carried out in live PTU-treated, and manually-dechorionated larvae at 24 hpf using the vital dye acridine orange (AO, #235474; Sigma-Aldrich, St. Louis, MO). Zebrafish embryos were incubated with 10 µg/mL AO solution for 15 min in the dark; the larvae were then washed three times with E3 medium. BODIPY™ 493/503 (D3922, Thermo Fisher Scientific, 100 µM) was used to stain neutral lipids in live zebrafish larvae. All images were acquired using a Leica M205FA stereo-microscope (Leica Microsystems), and fluorescence analysis was performed using Image-J software v.1.46, calculating the fluorescent intensity in the region of interest (ROI). All the ROIs used for the analysis were designed excluding the yolk/gut area and were localized in the brain (AO and BODIPY).

## Immunohistochemistry staining of whole-mount zebrafish embryos

Whole-mount immunohistochemistry was performed in 120 hpf embryos as described [20]. The primary antibodies used were: anti-ATP synthase subunit C (SCMAS) antibody (ab181243; Abcam, Cambridge, UK; 1;100) and anti-glial fibrillary acidic protein (GFAP) antibody (GTX128741; GeneTex, Irvine, CA; 1:100).

## Locomotor behavior and metformin treatment

Coiling behavior was measured to assess burst activity in homozygous *cln5*$^{-/-}$ and WT embryos at 30 hpf; to this end, the number of tail flicks in

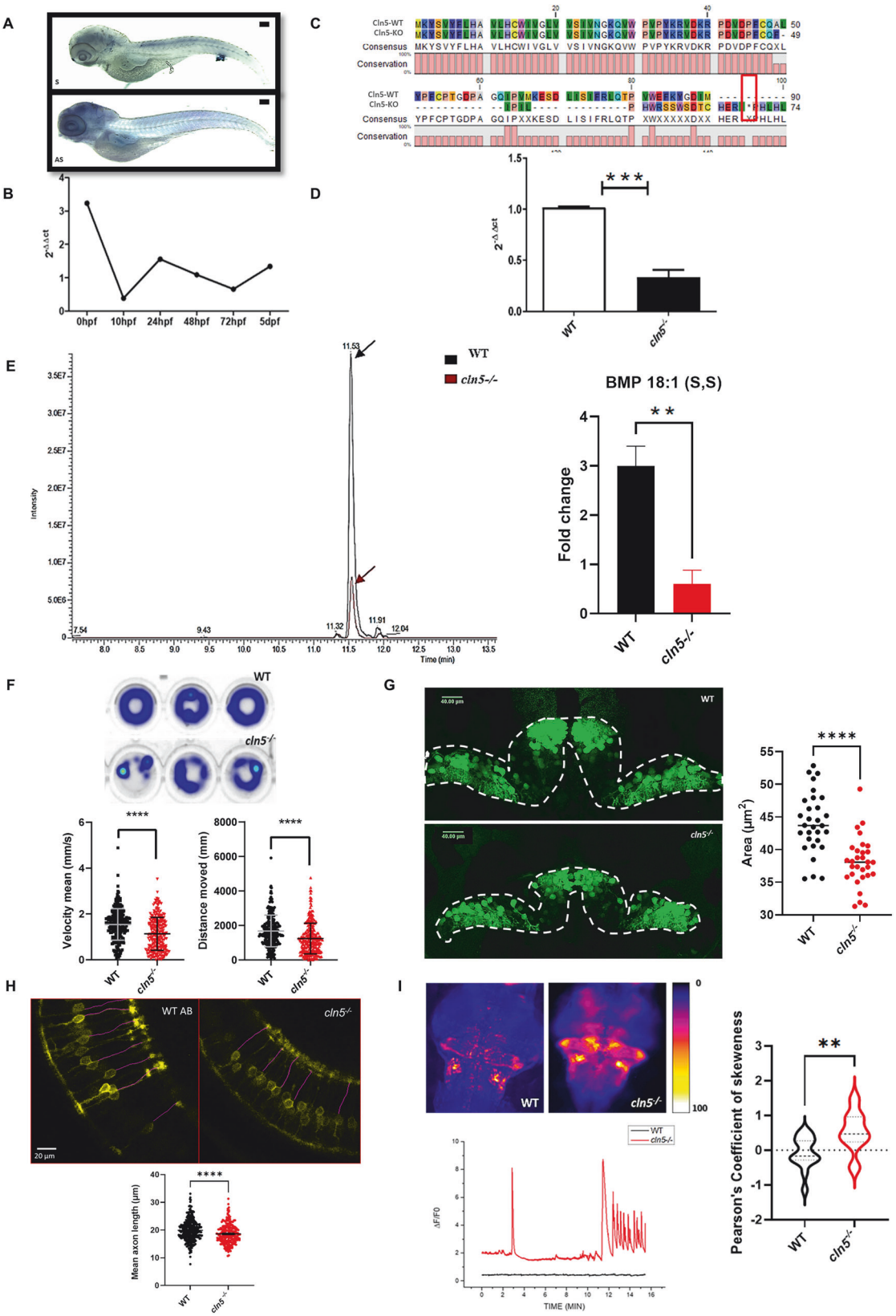


30 s was measured using a Leica M205FA stereo-microscope (Leica Microsystems) connected with Danioscope software (Noldus Information Technology). Larval locomotor behavior (distance travelled and velocity) was measured in homozygous *cln5*$^{-/-}$ larvae and WT larvae at 5 dpf using the DanioVision device (Noldus Information Technology BV; Wageningen, The Netherlands), and larval locomotor activity was recorded for 30 min and analyzed using EthoVision XT software (Noldus Information Technology BV; Wageningen, The Netherlands). Adult locomotor behavior was measured in homozygous *cln5*$^{-/-}$ and WT animals (12 months old, 50:50 male:female ratio) using the open field test as already described [20]. All trials were analyzed using Ethovision XT17 video-tracking software (Noldus Information Technology BV; Wageningen, The Netherlands), and distance

**Fig. 1 Characterization of the novel *cln5*$^{-/-}$ zebrafish mutant line. A** Whole mount in situ hybridization of the *cln5* transcript in 5 dpf larvae, showing the sense probe (S) and the antisense probe (AS). (scale bar = 100μm). **B** Temporal expression of *cln5* mRNA at different developmental stages using q-RT-PCR. **C** Protein alignment showing the early stop codon generated by CRISPR/cas9 system in mutant larvae (*cln5*$^{-/-}$) at position 69 (p.Ala49Phefs*69) compared to WT siblings. **D** The graph represents the decreased expression of *cln5* mRNA in mutant *cln5*$^{-/-}$ larvae at 5dpf compared to WT. The analysis was performed in triplicate using n = 30 for each experimental group. Statistical analysis has been performed using t-test (***P ≤ 0.001). **E** LC/MS dosage of BMP 18:1 (S,S) in adult brain of *cln5*$^{-/-}$ mutant (red line and arrow; n = 4) and WT zebrafish (black line and arrow; n = 4), showing a decreased BMP production in *cln5*$^{-/-}$, the graph shows the statistical analysis performed using t-test (**P ≤ 0.01). Areas are normalized on the signal of N,N-dimethylsphingosine (internal standard) **F** Locomotion analysis of 5 dpf WT and *cln5*$^{-/-}$ larvae. **G** Confocal images of the Purkinje cell layer, the graphs show the analysis of the area of the PCs layer in 5 dpf WT (*n* = 30) and *cln5*$^{-/-}$ (*n* = 30) larvae. All data were obtained from three independent experiments and were analyzed through statistical analysis (****P ≤ 0.0001) performed using the Mann-Whitney test. The values are expressed as mean ± standard error of the mean (SEM). **H** Analysis of axons length of retinal ON bipolar cells using confocal imaging, the graph shows a decreased length in *cln5*$^{-/-}$ (*n* = 39) compared to WT (*n* = 45), data were analyzed through statistical analysis (****P ≤ 0.0001) performed using the Mann-Whitney test. All data were obtained from three independent experiments. The values are expressed as mean ± standard error of the mean (SEM). **I** Representative z-projection images of the brain calcium imaging performed in the larvae in 16 min of recording, on the right there is the lookup table color range of calcium fluorescence. Analysis of calcium imaging analysis was performed by calculating Pearson's Coefficient of skewness in the two groups. Statistical analysis was performed using the Mann-Whitney test (****P ≤ 0.0001; **P ≤ 0.01). All data were obtained from three independent experiments. The values are expressed as mean ± standard error of the mean (SEM).

travelled and velocity were measured. Fifty 4 hpf embryos were randomly placed in 60 mm × 15 mm Petri dishes containing metformin (Sigma-Aldrich, St. Louis, MO) diluted in egg water to final working concentration of 50 μM. Stock solution was prepared in Milli-Q water (Merck-Millipore, Milan, Italy) and diluted in egg water. The media were not refreshed during the experiment unless otherwise stated.

### Electroretinogram recording (ERG)

ERG was performed on zebrafish (both *cln5*$^{-/-}$ and WT) at 5 dpf [35]. As described, a single eye of each individual fish was stimulated with flashes of 5 different light intensities, and the corresponding ERG b-wave amplitude was quantified.

### Simultaneous local field potential (LFP) and calcium imaging recordings and statistical analysis

Electrophysiological forebrain recordings were performed in 120 hpf zebrafish larvae to characterize epilepsy phenotype. The larvae were placed on a drop of 1.2% low melting point agarose and LFPs were recorded with an AgCl electrode inside a glass micropipette back loaded with 2 M NaCl. Electrophysiological signals were amplified 500-fold (EXT-02F, NPI, Tamm, Germany), band pass filtered (0.3–1300 Hz), and digitized at a rate of 5 kHz (Axon Digidata 1550B, Clampex 10.7.0.3, Molecular Devices, Berkeley, CA). The microelectrode was positioned by advancing its tip until it punctured the skin, after which it was carefully advanced into the forebrain. Data analyses of the LFP recordings were performed using a suite of custom MATLAB scripts. Burst activity analysis was performed on the LFP signals filtered in the 30–95 Hz band as already described. The root mean square (RMS) power of the signal was computed on the recording on rolling windows of 250 ms and in steps of 50 ms. Distributions were fitted with double Gaussians, then the ROC curves and areas under the curves were calculated; values > 0.9 were considered acceptable and events were extracted as described [22]. For normally distributed recordings, bursts were identified by extracting all events with a power higher than three standard deviations (SD) from the mean. Statistical analysis was performed using GraphPad Prism version 9 software (GraphPad Software Inc.). For calcium imaging analysis, zebrafish larvae at 120 hpf were restrained in low melting point agarose and a Nikon FN1 microscope (Nikon, Tokyo, Japan) was used for video recording; the image acquisitions were obtained using a Prime sCMOS camera (Teledyne Photometrics, Tucson, AZ) supplied with Metafluor software (Molecular Devices, San Jose, CA), applying a time-lapse interval of 150 ms and acquiring 3860 frames per video. The distribution of fluorescence fluctuations (ΔF/F0) in the brain area was evaluated in a pre-defined ROI using ImageJ 64 software. Data were normalized to background fluorescence and were quantified by the Pearson's coefficient of skewness, as described elsewhere [36].

### Patients

One patient with a clinical and genetic diagnosis of *CLN5* and two with *CLN7* were recruited from the participating members of CLNet, the Italian network on NCL. In accordance with the Declaration of Helsinki, all study participants provided written informed consent for a skin biopsy as part of routine diagnostic procedures.

### Cell cultures

Fibroblasts were isolated from skin biopsies of 3 affected patients and 3 healthy controls. Cells were cultured at 37 °C with 5% CO2 in Dulbecco's Modified Eagle's Medium (DMEM), supplemented with 10% fetal bovine serum, 4.5 g/L glucose, and 1% antibiotics/antimycotics. Primary fibroblasts from CLN5 patients Pt2 and Pt3 (genotype and phenotype features were reported in [37]) were treated with metformin (Sigma Aldrich) 500uM, 24 h in regular growth medium at 37 °C in 5% CO2.

### Statistics

All data in the manuscript represent three or more independent experiments. Statistical analysis was performed using GraphPad Prism 6. All quantitative variables were initially assessed for normality using the Shapiro-Wilk test. Based on the normality test results, either parametric or non-parametric methods were applied. For comparisons between two different groups the analysis was performed using the T-test for normally distributed data. In cases where the data did not pass the normality test, the non-parametric Mann-Whitney test was applied to compare distributions between the groups. For multiple comparisons, Dunn's test was performed after the Kruskal-Wallis test, since the data of the various groups examined did not show Gaussian distribution. Statistical significance is reported as follows: $*p \le 0.05$, $**p \le 0.01$, $***p \le 0.001$, or $****p \le 0.0001$. The specific test applied for each analysis is reported in the figure legend.

## RESULTS

### Generation and characterization of novel *cln5*$^{-/-}$ zebrafish line

We evaluated the spatiotemporal expression of *cln5* during zebrafish development. In situ hybridization of *cln5* mRNA revealed that it is expressed over the entire larval body at 5 dpf with highest expression at brain level (Fig. 1A). We found it to be expressed from the first stage of development (it is highly expressed at 0 hpf); after midblastula transition at 10 hpf its expression decreases and thereafter it is constantly expressed until 5 dpf (Fig. 1B). We successfully edited the novel *cln5*$^{-/-}$ zebrafish model using the CRISPR/Cas9 system, which resulted in a 2-bp deletion and a missense mutation in exon 2. This led to a frameshift mutation and an early stop codon at residue 69 (Fig. 1C). The efficacy of the mutation was further confirmed by qRT-PCR analysis in homozygous F2 mutant *cln5*$^{-/-}$ larvae, which showed reduced expression of *cln5* mRNA versus control siblings (Fig. 1D), likely as a consequence of nonsense-mediated mRNA decay (NMD). We further confirmed gene depletion by performing mass spectrometry assessment of BMP production, detecting a high decrease of (18:1/18:1) BMP (S,S) in *cln5*$^{-/-}$ mutant larvae as compared to WT controls (Fig. 1E). Additionally, we also observed a decrease of BMP 22:6, 22:6, which is among the most abundant in the brain, and an increase of LPG the precursor of BMP (Supplementary Figure 1A). The mutation did not affect viability,

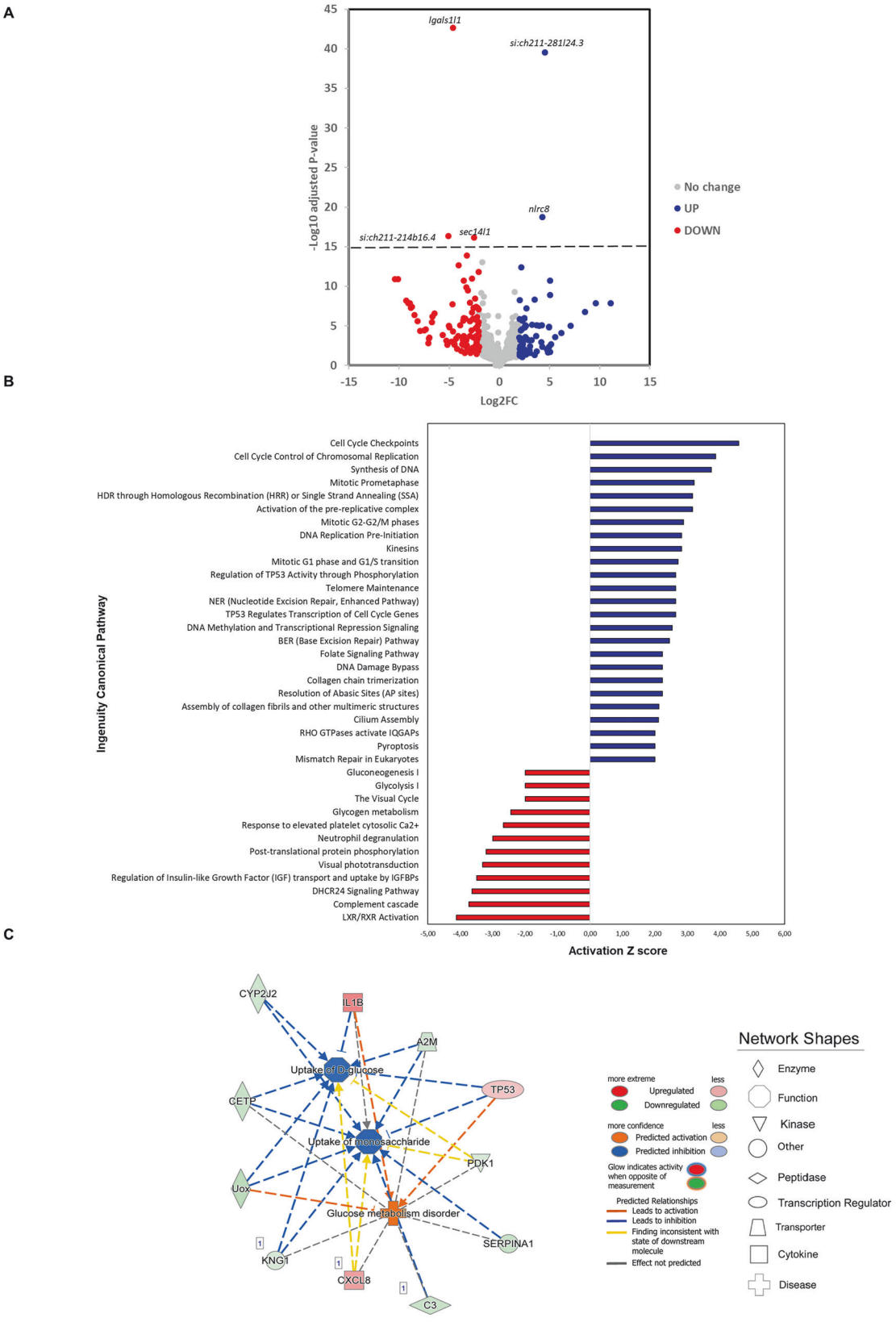


**Fig. 2 Transcriptomic analyses of whole larvae. A** Volcano plot. The log2 FC indicates the mean expression level for each gene. Each dot represents one gene. The names near the dots indicate the genes with values with a log10 of adjusted p-value major than 15, the dotted line represents a threshold settled at 15. **B** RNA-seq analysis performed on 5 dpf larvae, the graph showed the canonical pathways altered in *cln5*$^{-/-}$ mutant compared to WT. The analysis has been performed using maximal stringency with p value < 0.01 and z score >2 and <−2. **C** Two distinct networks were reconstructed to be involved in Glucose Metabolism (Focused Molecules $n = 11$).

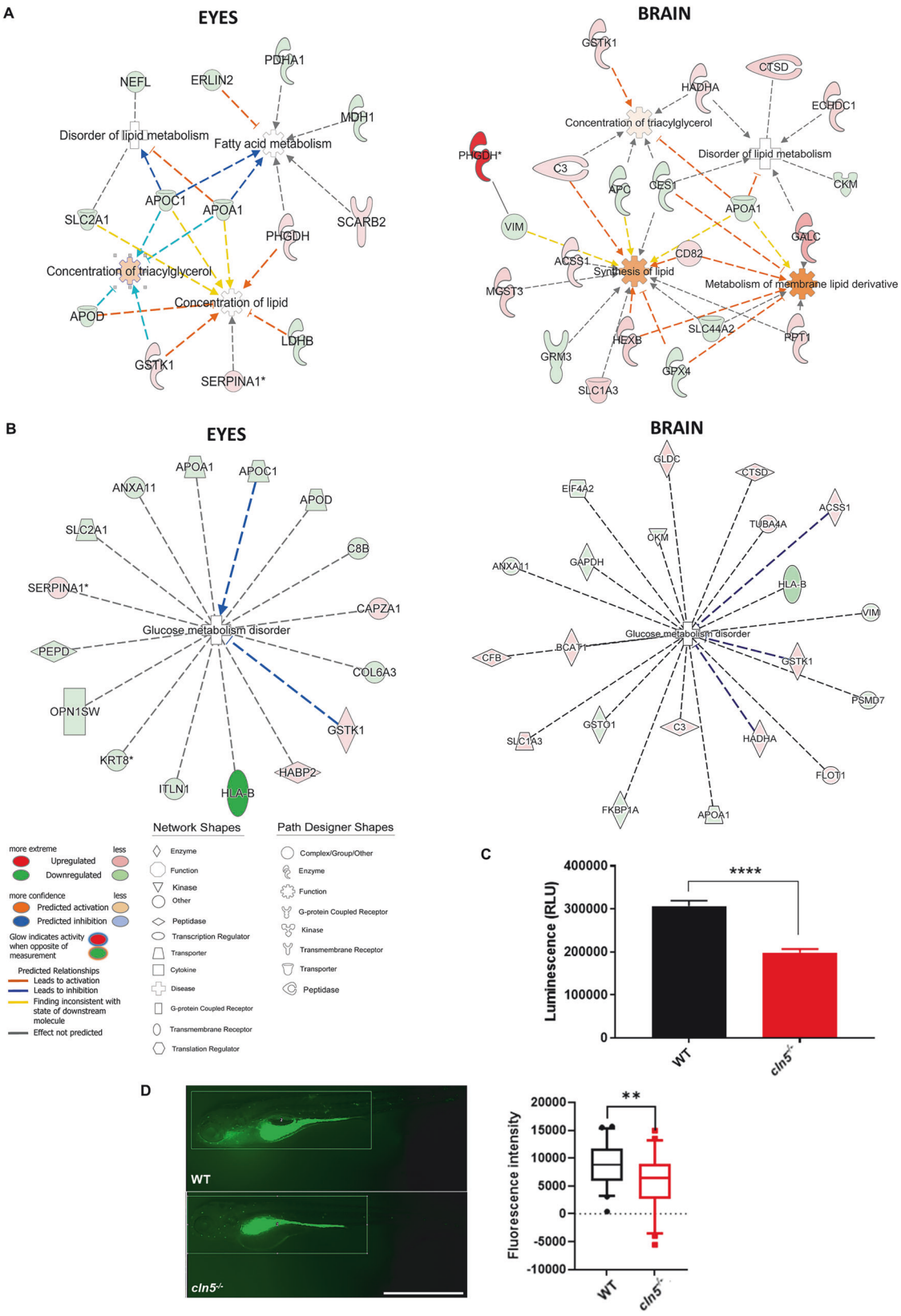


and the Mendelian ratios were maintained. We also observed no qualitative difference in the phenotype between zygotic *cln5*$^{-/-}$ embryos derived from heterozygous females and maternal-zygotic (MZ) *cln5*$^{-/-}$ embryos obtained from homozygous mutant females. This finding suggests that maternal *cln5* mRNA does not play a crucial role during early embryonic development in zebrafish. Morphological analyses of 5 dpf larvae showed that the mutant larvae had a slightly increased body length, and an increased yolk sac area (Supplementary Figure 1B). Moreover, our novel *cln5*$^{-/-}$ mutants recapitulate the main pathological features

**Fig. 3 Proteomic analyses of isolated brains and eyes of adult fish using IPA software. A** The networks in both brain and eyes show alterations in lipid metabolism. **B** The networks portraying the DEPs involved in altered glucose metabolism. **C** The graph represents the glucose uptake assay in *cln5*$^{-/-}$ and WT 96 hpf larvae. The values are expressed as mean ± standard error of the mean (SEM). Statistical analysis was performed using the Mann-Whitney test (****P ≤ 0.0001). **D** In vivo glucose uptake analysis using 2-NBDG, figure show images of zebrafish larvae at 5 dpf (scale bar 1000 μm), the rectangle indicate the ROI used for the analysis of fluorescence intensity, the graph showed the quantification of fluorescence intensity in n = 45 *cln5*$^{-/-}$ and WT respectively. The values are expressed as mean ± standard error. Statistical analysis was performed using the Mann-Whitney test (**P ≤ 0.01). All data were obtained from three independent experiments.

of the NCL disease, displaying accumulation of subunit C of mitochondrial ATP synthase (SCMAS) (Supplementary Figure 1C), increased apoptosis in the brain (Supplementary Figure 1D), and lipid accumulation in the larval brain (Supplementary Figure 1E), although the increase and fold change are not as pronounced, possibly due to the progressive nature of lipid accumulation in CLN5 impairment. Mutant embryos and larvae demonstrated an altered behavior associated with increased tail coiling, related to increased hyperexcitability (Supplementary Figure 1F), with reduced locomotor performances in distance and velocity travelled both in larvae (Fig. 1F) and adult mutants when compared to WT (Supplementary Figure 1G). Since Purkinje cells (PCs) are the most affected neuronal cells in the brain of NCL patients and animal models [38, 39], we used the transgenic strain *Tg(aldoca:GAL4FF)* to analyze the PCs, and observed decreased PCs layer compared to WT siblings (Fig. 1G).

We evaluated the effect of Cln5 loss of function on retinal function, since blindness is a feature of NCL disease, and observed that our *cln5*$^{-/-}$ model showed a decreased b-wave amplitude to high intensity light stimuli (Supplementary Figure 2A), which was further confirmed through behavioral analysis performed using an optokinetic response test, demonstrating a decreased number of saccades in *cln5*$^{-/-}$ mutants compared to WT siblings (Supplementary Figure 2B). To further confirm the retinal dysfunction we used the transgenic line *Tg(nyx:mYFP)* tagging retinal ON-bipolar cells, and showed that *cln5* depletion causes a decrease in axonal length of retinal cells (Fig. 1H). The use of the *Tg (neurod1:G-CaMP6F)* transgenic line allowed to reveal that *cln5*$^{-/-}$ mutant larvae have increased neuronal excitability, exhibiting "seizures-like events" on LFP recordings (Supplementary Figure 2C), with higher power and duration compared to WT (Supplementary Figure 2D). Calcium imaging recordings showed that the loss of Cln5 induced an impairment of calcium homeostasis in zebrafish neurons, with a higher increase of calcium flux in mutants as compared to control siblings, mainly at the hindbrain level. While some changes were also observed in forebrain neurons, the alterations were not as clearly defined as those in the hindbrain (Fig. 1I, Supplementary Video 1, 2).

Since CLN5 dysfunction, together with other forms of NCLs, showed altered mitochondrial function, autophagy and increased inflammation we analyzed these molecular pathways in our in vivo model, confirming that it recapitulates at the molecular level the characteristics of NCL dysfunction. We observed decreased mitochondrial function associated with decreased basal respiration rate, maximal respiration rate, and ATP production (Supplementary Figure 3A). Furthermore, our *cln5*$^{-/-}$ mutants showed increased gene expression of several inflammatory factors such as *tnfa*, *il1β*, *p2ry12* and *gfap* (Supplementary Figure 3B), indicating elevated inflammation, which was validated by immunofluorescence using anti-glial fibrillary acidic protein (GFAP) antibody, demonstrating that Gfap was overexpressed in *cln5*$^{-/-}$ brain compared to WT larvae (Supplementary Figure 3C). Similarly, the autophagy pathway seemed impaired in mutant larvae, indeed some of the most important genes involved in autophagy were upregulated compared to control larvae (Supplementary Figure 3D). Autophagic impairment was confirmed through western blotting, in which we observed an increased ratio of LC3II/LC3I in *cln5*$^{-/-}$, a marker of autophagosome, and an enhanced expression of LAMP1, a marker for lysosomes (Supplementary Figure 3E).

### Transcriptomic analysis suggests possible impairment in lipid and glucose metabolisms

RNA-seq analyses showed 76 upregulated and 101 downregulated genes in *cln5*$^{-/-}$ larvae compared to WT (Fig. 2A). Canonical pathway analysis using Ingenuity Pathway Analysis (IPA) revealed that most of the DEGs in mutants compared to WT were associated with apoptosis, visual function, and cell cycle, while the most downregulated pathways were linked to glucose metabolism, such as the regulation of insulin growth factor (IGF) transport and uptake, glycolysis and gluconeogenesis (Fig. 2B; Supplementary Table 2). IPA analyses indicate that *cln5*$^{-/-}$ larvae exhibited reduced glucose uptake and potential disruptions in glucose metabolism (Fig. 2C). Expectedly, altered lipid metabolism constituted an additional pathway differentially regulated in mutant larvae (Supplementary Figure 4A), and these findings were further confirmed by the specific BODIPY staining analysis for lipid accumulation in Supplementary Figure 1D. We observed an accumulation of lipids in the brains of zebrafish larvae (Supplementary Figure 1D), and a decrease in the synthesis of BMP lipid (Fig. 1E).

### Proteomic analysis at different developmental stages of *cln5*$^{-/-}$ mutant zebrafish

Proteomic analyses at different developmental stages (namely, 6 hpf and adult brain and eyes) showed several DEPs in our *cln5*$^{-/-}$ samples compared to WT (Supplementary Table 3). IPA analyses on adult brain and eye samples (Supplementary Table 3), support the RNA-seq results, indicating alterations in both lipid metabolism (Fig. 3A) and glucose metabolism (Fig. 3B), in both the brain and eyes being the most statistically significant. To confirm the results on altered glucose metabolism we performed a glucose uptake assay, which demonstrated a profound decrease in glucose uptake in *cln5*$^{-/-}$ larvae compared to the WT ones (Fig. 3C, D), thereby functionally validating the transcriptomic and proteomic data.

### Identification of novel cross-species biomarker relevant for different NCLs forms

We combined the DEPs identified in adult and embryos samples in order to highlight common biomarkers (Fig. 4A). The analysis showed that phosphoglycerate dehydrogenase (PHGDH) was overexpressed in all three samples (Fig. 4B). By western blotting we confirmed an overexpression of Phgdh in larval (Fig. 4C) and adult brain zebrafish samples (Fig. 4D), which has been further validated in human cells derived from three patient carrying the *CLN5* mutations p.Trp224*/p.Val263Glu (CLN5-Pt1), p.Tyr258Asp/p.Tyr258Asp (CLN5-Pt2), and p.Arg199*/p.Arg199* (CLN5-Pt3) (Fig. 4E, F), with the CLN5-Pt3 cell line displaying a reduction in PHGDH protein levels (Fig. 4F). Moreover, it was replicated in two NCL patients carrying homozygous mutations c.863+4 A > G (CLN7-Pt1); p.Arg139His (CLN7-Pt2)) in *CLN7* (Fig. 4G).

### Metformin treatment rescues PHGDH expression in human fibroblast and behavioral deficits in zebrafish

In order to identify a possible modulator of glucose metabolism we performed a treatment with metformin on CLN5 human fibroblasts of CLN5-Pt2 and CLN5-Pt3, showing that the treatment is able to restore the expression of PHGDH (Fig. 5A, B). Moreover, the treatment of zebrafish embryos confirmed the rescue effect of metformin on impaired coiling behavior in mutant embryos (Fig. 5C).

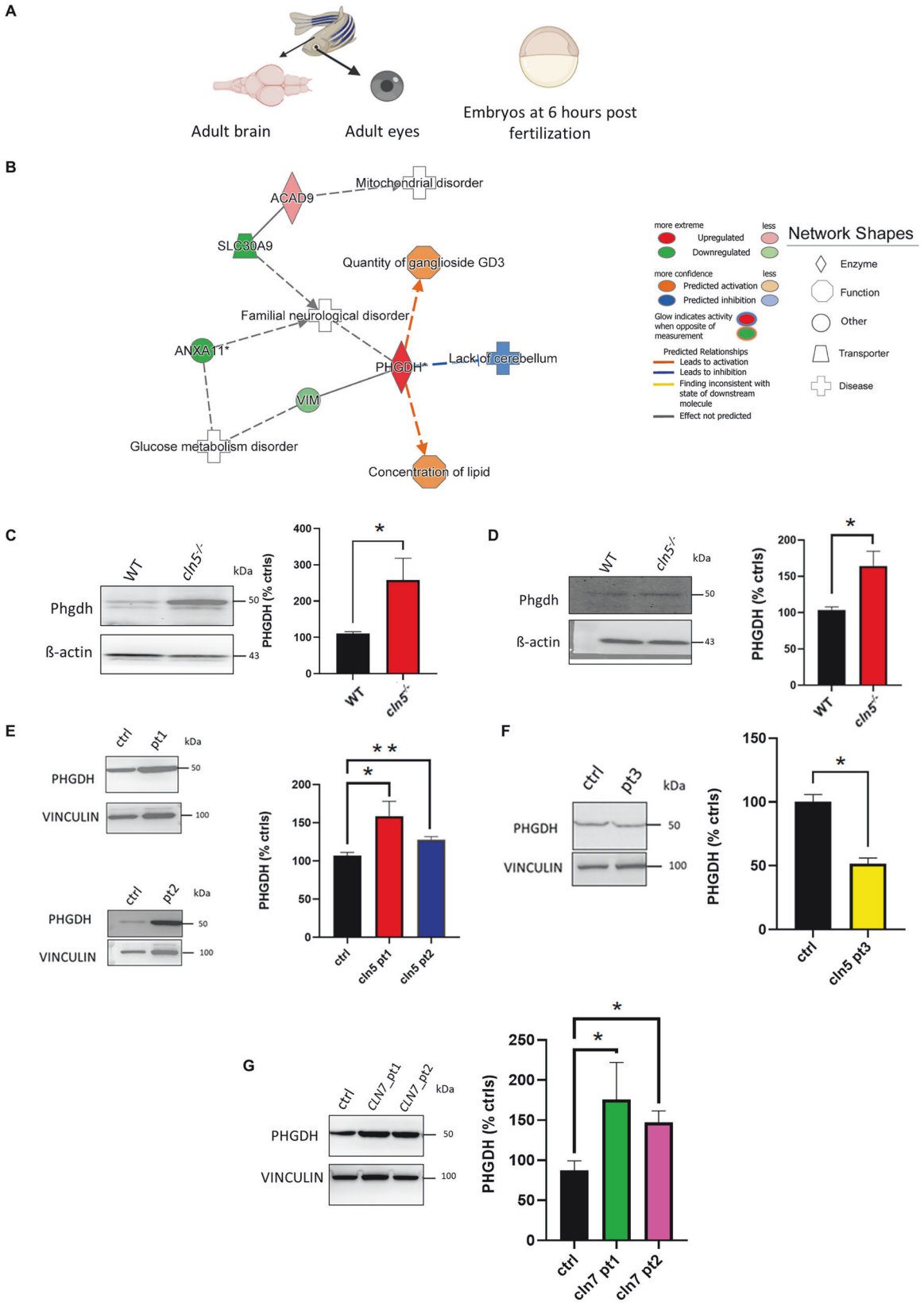


## DISCUSSION

The limited understanding of CLN5-related cellular mechanisms and lack of defined pharmacological targets underscore the need to study the developmental impact of CLN5 loss, with a focus on uncovering pathways and biomarkers relevant to juvenile dementia [2]. Our novel zebrafish *cln5*$^{-/-}$ model recapitulates the main features of the late-infantile form of Batten disease [37], including decreased BMP synthesis [11], increased cell death,

**Fig. 4 Biomarker identification and validation. A** Schematic representation of samples analyzed through comparative analysis. **B** Comparative proteomic analysis showing common DEPs, such as SLC30A9; ANXA11 and PHGDH. **C** Western blotting of Phgdh in zebrafish larvae, revealing an increased expression in mutant *cln5*$^{-/-}$. **D** Western blotting of Phgdh in adult zebrafish brain, revealing an increased expression in mutant *cln5*$^{-/-}$. **E, F** Western blotting analysis of human PHGDH in patients' fibroblasts carrying the *CLN5* mutations. **G** Western blotting analysis of human PHGDH in two patients' fibroblasts carrying the *CLN7* mutations. Protein's levels were normalized to ß- actin or vinculin. Values represent the mean ± standard error of the mean (SEM), with n ≥ 3 for each group with 40/50 larvae per sample. Mann-Whitney test and Student's t-test were performed using (*P ≤ 0.05; **P ≤ 0.01).

accumulation of subunit C of ATP synthase, "ataxia-like" motor behavior, vision loss and "seizures-like" events. Moreover, in-depth characterization also revealed retinal degeneration and decreased axonal length [40], in ON-bipolar cells, resembling the dysfunction already observed in the CLN5 KO ovine model [41]. These parallels make the *cln5*$^{-/-}$ zebrafish a powerful tool for studying the neurodegenerative progression in CLN5 disease, especially in early-life stages, to better understand the cellular changes contributing to juvenile dementia. Interestingly, a decreased PCs layer has also been observed upon *cln5* depletion, a finding common to other NCLs forms [39], which is further supported by an increased apoptosis in the brain at early stages (24 hpf). Taken together, our gene editing and follow-up characterization in zebrafish offers a new tool to investigate CLN5-related pathology during early development. As observed in similar NCL models [20, 42], zebrafish strains are particularly amenable for drug screening or repurposing. Three additional points of interest emerged from the current study. First, we uncovered the potential role of CLN5 in calcium homeostasis. Indeed, analysis of the brain function with calcium imaging recordings and the *Tg(neurod1:GCaMP6F)* transgenic line revealed an impaired calcium homeostasis in the brain, mostly localized in the cerebellum, which is in line with what has been previously reported for other ions, but not calcium, in *Cln5*$^{-/-}$ mice model, suggesting that disrupted calcium homeostasis may drive neurodegeneration and cellular stress in CLN5-related juvenile dementia [5]. The previous interactomics studies suggested that CLN5 binds to several calcium-regulated proteins (i.e. calnexin, calumenin, calreticulin, calreticulin 3) [43–45]. This finding indicates a potential role of CLN5 in calcium homeostasis and release, both of which may have a role in neuronal hyperexcitability. It may underline a defect of glia-neuron crosstalk in consideration of the documented impairment of calcium signaling in primary astrocytes derived from *Ppt1*$^{-/-}$ and *Cln3*$^{-/-}$ mice [10, 46]. In our zebrafish model study, we observed an increased expression of neuroinflammation markers, *tnfa* and *il1β*, and increased expression of *gfap* in the brain, suggestive for astrogliosis as shown in mouse model [47]. This neuroinflammatory response may contribute to the cognitive and behavioral symptoms seen in pediatric dementia by accelerating neuronal dysfunction.

Second, in our *cln5*$^{-/-}$ model we could recapitulate autophagic defects that were observed in vitro in neuronal-like human cells [32], thus bridging the gap between animal and human cell models. Altered autophagy pathway linked to increased expression of the key proteins, such as Lamp1 (lysosomal marker) and Lc3II/Lc3I ratio (autophagosome marker) in our zebrafish model suggests a compromising cargo degradation with dysregulated autophagosome-lysosome fusion in mutant fish. This impairment likely contributes to neurodegeneration and cognitive decline in juvenile dementia, as autophagy is critical for maintaining neuronal health. Therapeutic targeting of autophagy in CLN5 and other NCLs may therefore represent a promising strategy for slowing disease progression and ameliorating dementia symptoms in affected children.

Third, and importantly, we performed multi-omics studies in larvae and adult brains and eyes disclosing, at different developmental stages (embryos and adults) the same differentially abundant proteins (i.e. Ctsd, Hexb), already pinpointed by lysosomal-targeted organelle proteomics in SHSY-5Y KO *CLN5* [12]). These data point to the already observed lysosomal-autophagy balance and lipid metabolism [12, 48], suggesting the zebrafish KO strain to be sufficiently robust to model the human disease status. Original data pointed to alteration in glucose metabolism with decreased uptake of glucose, which has been assorted to *cln5* dysfunction for the first time, though a hint to this information had been partially presented by others [49, 50]. Furthermore, we observed a predicted downregulation of the pathway related to insulin growth factor 1 (IGF1) transport and uptake, which can be considered as a potential drug target for CLN5 and other NCLs forms, as seen in *mnd/mnd* mouse model [51]. This metabolic disruption resembles energy imbalances reported in other neurodegenerative diseases and could underlie dementia-related symptoms such as memory loss and executive dysfunction. Scrutinizing the proteomic analyses in early development (6 hpf embryos) and later stages (adult fish) we paid attention to PHGDH, a marker of phosphoserine pathway. We also confirmed a differential expression of Phgdh in zebrafish samples and its cross-species validation in primary skin fibroblasts from three patients harboring different mutations in *CLN5*. Our analysis revealed that two patients, Pt1 and Pt2, exhibited increased expression levels of PHGDH. In contrast, the third patient, Pt3, demonstrated a decreased expression of PHGDH. This variation may be attributed to the distinct types of genetic mutations present in each patient, as well as differences in the levels of CLN5 protein expression. Notably, as previously reported by [37], Pt3 showed a complete absence of CLN5 protein signal in Western blot analysis compared to Pt1 and Pt2, which may further explain the observed decrease in PHGDH expression. Interestingly, both Pt2 and Pt3, as preliminary data, responded to metformin treatment, which restored PHGDH expression. Metformin is well known for its effects on cellular metabolism, particularly in regulating mitochondrial function, autophagy, and glucose homeostasis. In the context of CLN5 deficiency, which impairs lysosomal function and contributes to neurodegeneration, its mechanism of action could offer an intriguing therapeutic opportunity. By acting on complex I of the mitochondrial respiratory chain, metformin reduces oxidative stress and enhances energy efficiency [52], counteracting the energy deficits characteristic of mitochondrial dysfunction associated with CLN5 deficiency [32]. Additionally, its ability to activate AMPK promotes the autophagic process, facilitating the removal of damaged proteins and organelles [53]. This may help to alleviate the accumulation of toxic aggregates, a central feature of neurodegenerative diseases linked to CLN5 [16].

Another important aspect to consider is metformin's effect on glucose metabolism. While primarily used to treat type 2 diabetes, its impact on metabolic homeostasis extends to the nervous system, where maintaining a proper energy balance is crucial for neuronal survival and function. By stabilizing glucose metabolism, metformin could strengthen neuronal resilience against metabolic disturbances caused by CLN5 deficiency [54].

These properties suggest that metformin may have a protective role in conditions associated with CLN5 deficiency, mitigating cellular damage by improving mitochondrial function, activating autophagy, and regulating metabolism. Although further research is needed to confirm these effects in

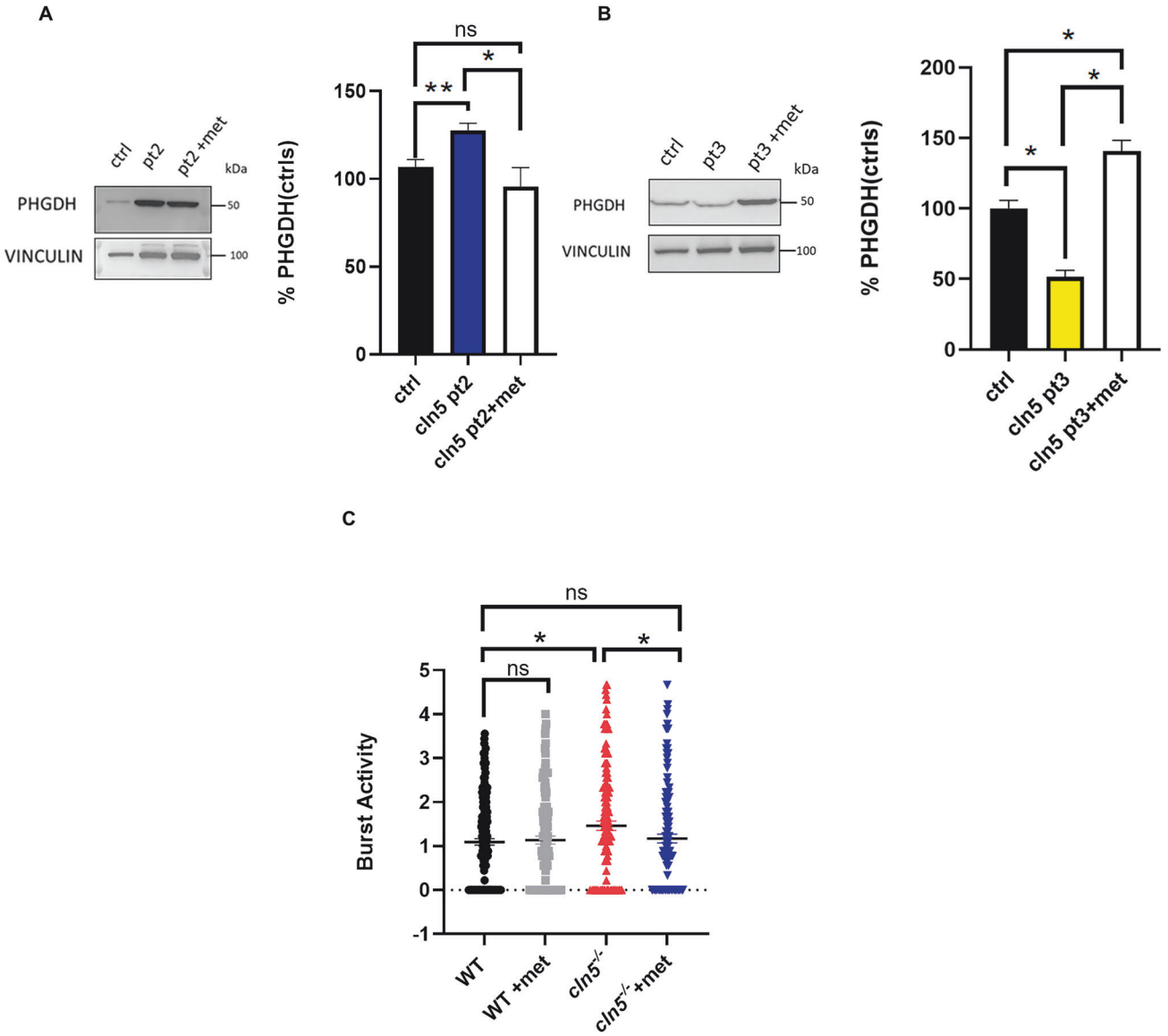


**Fig. 5 Metformin treatment on human CLN5 fibroblasts and cln5$^{-/-}$ zebrafish. A** Western blot assay of CLN5 Pt2 fibroblasts treated with metformin. **B** Western blot assay of CLN5 Pt3 fibroblasts treated with metformin. Protein's levels were normalized to vinculin. Mann-Whitney test was performed using (*P ≤ 0.05; **P ≤ 0.01). **C** Analysis of coiling behavior in *cln5*$^{-/-}$ and WT 30 hpf embryos after treatment with metformin. Statistical analysis was performed using the Mann-Whitney test (*p ≤ 0.05).

experimental and clinical models, its ability to modulate key biological processes makes metformin a promising candidate for therapeutic strategies targeting lysosomal storage disorders and related neurodegenerative diseases. However, the precise molecular mechanism linking CLN5 deficiency to metformin remains to be fully elucidated. Given CLN5's role in lysosomal function and metabolic regulation, metformin's ability to restore PHGDH levels highlights a potential connection between CLN5 dysfunction and serine biosynthesis. This finding suggests that PHGDH could serve as a valuable biomarker for evaluating treatment responses, indicating its potential role in therapeutic strategies targeting this pathway. Future studies using patient-derived iPSCs reprogrammed into neurons could provide further insights into disease mechanisms and metformin's mode of action in this context. Furthermore, increased expression of PHGDH has been confirmed also in two patients carrying *CLN7* mutations, confirming that this protein may also be considered a biomarker for other Batten disease subtypes. The latter finding could be related to the work of López-Fabuel and colleagues [55], who presented an aberrant upregulation of the glycolytic enzyme PFKFB3 in CLN7, showing that in certain conditions, there is a shift in cellular metabolism towards glycolysis, demonstrating that it contributes to the progression of neurodegeneration by affecting energy production, redox balance, and cell survival mechanisms. Given these findings, the overexpression of PHGDH in CLN7 could be part of a broader metabolic dysregulation repertoire similar to what has been observed by López-Fabuel and colleagues.

It is hard to imagine, at this stage, the mechanistic relevance of PHGDH in CLN5 disease and in other NCLs forms, such as CLN7. We speculate that PHGDH may interact with some NCLs proteins, since from a comparison study on three interactomes, PHGDH has been found to interact with CLN3 and CLN5 [43, 56], suggesting that it may play an important role in the NCL-causative pathways. Moreover, an overexpression of PHGDH, which catalyzes the first step in serine biosynthesis pathway, could play a role in NCLs through alteration of serine and glycine levels, leading to altered cellular metabolism and

neurotransmitter balance, and contributing to neurodegenerative processes observed in NCLs via neuronal dysfunction and enhanced oxidative stress. Overexpression of PHGDH might also induce alterations in lipid metabolism, since serine is a precursor for sphingolipids and phosphatidylserine, leading to abnormal accumulation or altered composition of lipids within neuronal cells. This disturbance could contribute to the formation of lipofuscin deposits characteristic of NCLs. Furthermore, PHGDH plays an important role in neurotransmitter synthesis (e.g., D-serine as a co-agonist at NMDA receptors), therefore its overexpression may affect synaptic function and plasticity. Indeed, impaired neurotransmission is a significant feature of NCLs [57]. In this regard, PHGDH overexpression has been already denoted as a biomarker of progression in Alzheimer's disease [58], and selective expression of the protein in astrocytes, can influence the role of serine metabolism in glial-neuronal communication, offering new opportunities to monitor and target the disease status [59]. Further research is required to clarify these potential links and to explore therapeutic strategies targeting PHGDH-related pathways in NCLs. Given PHGDH's role in both metabolic and synaptic processes, this biomarker could also inform personalized treatment approaches for juvenile dementia symptoms, including cognitive and motor impairments.

In summary, the development of this innovative in vivo model of CLN5 offers a groundbreaking platform that faithfully mimics the behavioral, physiological, and molecular characteristics of CLN5 disease. This model not only opens new avenues for exploring the novel functions of the CLN5 protein in axonal growth and calcium homeostasis within the brain but also sheds light on an altered glucose metabolism linked to CLN5 loss-of-function. Such insights could lead to exciting new strategies to halt or delay the progression of CLN5-related human disease. By identifying PHGDH as a biomarker and demonstrating the therapeutic potential of metformin, this study contributes valuable insights for future research and treatment strategies targeting the neurodegenerative and psychiatric features of NCLs. This discovery positions PHGDH as a potential target for innovative therapeutic approaches in NCLs.

## DATA AVAILABILITY

The data that support the findings of this study are available from the corresponding author, upon reasonable request. All data generated or analyzed during this study are included in this published article and its Supplementary Information Files. Mass spectrometry data were deposited in the Mass Spectrometry Interactive Virtual Environment (MassIVE) database under accession number MSV000095679. RNA-seq data were deposited in Zenodo https://doi.org/10.5281/zenodo.15057134.

## REFERENCES

1. Santorelli FM, Garavaglia B, Cardona F, Nardocci N, Bernardina BD, Sartori S, et al. Molecular epidemiology of childhood neuronal ceroid-lipofuscinosis in Italy. Orphanet J Rare Dis. 2013;8:19.
2. Gardner E, Mole SE. The genetic basis of phenotypic heterogeneity in the neuronal ceroid lipofuscinoses. Front Neurol. 2021;12:754045.
3. Mole SE, Anderson G, Band HA, Berkovic SF, Cooper JD, Kleine Holthaus SM, et al. Clinical challenges and future therapeutic approaches for neuronal ceroid lipofuscinosis. Lancet Neurol. 2019;18:107–16.
4. Holmberg V, Jalanko A, Isosomppi J, Fabritius AL, Peltonen L, Kopra O. The mouse ortholog of the neuronal ceroid lipofuscinosis CLN5 gene encodes a soluble lysosomal glycoprotein expressed in the developing brain. Neurobiol Dis. 2004;16:29–40.
5. Basak I, Wicky HE, McDonald KO, Xu JB, Palmer JE, Best HL, et al. A lysosomal enigma CLN5 and its significance in understanding neuronal ceroid lipofuscinosis. Cell Mol Life Sci. 2021;78:4735–63.
6. Magliyah MS, Geuer S, Alsalamah AK, Lenzner S, Drasdo M, Schatz P. Association of the recurrent rare variant c.415T>C p.Phe139Leu in CLN5 with a recessively inherited macular dystrophy. JAMA Ophthalmol. 2021;139:339–43.
7. Mancini C, Nassani S, Guo Y, Chen Y, Giorgio E, Brussino A, et al. Adult-onset autosomal recessive ataxia associated with neuronal ceroid lipofuscinosis type 5 gene (CLN5) mutations. J Neurol. 2015;262:173–8.
8. Baeza MR, Solé J, León A, Arraztoa J, Rodríguez R, Claure R, et al. Conservative treatment of early breast cancer. Int J Radiat Oncol Biol Phys. 1988;14:669–76.
9. Qureshi YH, Patel VM, Berman DE, Kothiya MJ, Neufeld JL, Vardarajan B, et al. An Alzheimer's disease-linked loss-of-function CLN5 variant impairs cathepsin D maturation, consistent with a retromer trafficking defect. Mol Cell Biol. 2018;38:e00011–18.
10. Lange J, Haslett LJ, Lloyd-Evans E, Pocock JM, Sands MS, Williams BP, et al. Compromised astrocyte function and survival negatively impact neurons in infantile neuronal ceroid lipofuscinosis. Acta Neuropathol Commun. 2018;6:74.
11. Medoh UN, Hims A, Chen JY, Ghoochani A, Nyame K, Dong W, et al. The Batten disease gene product CLN5 is the lysosomal bis(monoacylglycero)phosphate synthase. Science (New York, N.Y.). 2023;381:1182–9.
12. Doccini S, Marchese M, Morani F, Gammaldi N, Mero S, Pezzini F, et al. Lysosomal proteomics links disturbances in lipid homeostasis and sphingolipid metabolism to CLN5 disease. Cells. 2022;11:1840.
13. Käkelä R, Somerharju P, Tyynelä J. Analysis of phospholipid molecular species in brains from patients with infantile and juvenile neuronal-ceroid lipofuscinosis using liquid chromatography-electrospray ionization mass spectrometry. J Neurochem. 2003;84:1051–65.
14. Miranda AM, Lasiecka ZM, Xu Y, Neufeld J, Shahriar S, Simoes S, et al. Neuronal lysosomal dysfunction releases exosomes harboring APP C-terminal fragments and unique lipid signatures. Nat Commun. 2018;9:291.
15. Gomes S, Garrido A, Tonelli F, Obiang D, Tolosa E, Martí MJ, et al. Elevated urine BMP phospholipids in LRRK2 and VPS35 mutation carriers with and without Parkinson's disease. NPJ Parkinsons Dis. 2023;9:52.
16. Medoh UN, Abu-Remaileh M. The Bis(monoacylglycero)-phosphate hypothesis: from lysosomal function to therapeutic avenues. Annu Rev Biochem. 2024;93:447–69.
17. Mahmood F, Fu S, Cooke J, Wilson SW, Cooper JD, Russell C. A zebrafish model of CLN2 disease is deficient in tripeptidyl peptidase 1 and displays progressive neurodegeneration accompanied by a reduction in proliferation. Brain. 2013;136:1488–507.
18. Kim WD, Wilson-Smillie MLDM, Thanabalasingam A, Lefrancois S, Cotman SL, Huber RJ. Autophagy in the neuronal ceroid lipofuscinoses (Batten Disease). Front Cell Dev Biol. 2022;10:812728.
19. Heins-Marroquin U, Singh RR, Perathoner S, Gavotto F, Merino Ruiz C, Patraskaki M, et al. CLN3 deficiency leads to neurological and metabolic perturbations during early development. Life Sci Alliance. 2024;7:e202302057.
20. Marchese M, Bernardi S, Ogi A, Licitra R, Silvi G, Mero S, et al. Targeting autophagy impairment improves the phenotype of a novel CLN8 zebrafish model. Neurobiol Dis. 2024;197:106536.
21. Rupprecht P, Prendergast A, Wyart C, Friedrich RW. Remote z-scanning with a macroscopic voice coil motor for fast 3D multiphoton laser scanning microscopy. Biomed Opt Express. 2016;7:1656–71.
22. Della Vecchia S, Ogi A, Licitra R, Abramo F, Nardi G, Mero S, et al. Trehalose treatment in zebrafish model of lafora disease. Int J Mol Sci. 2022;23:6874.
23. Walker SL, Ariga J, Mathias JR, Coothankandaswamy V, Xie X, Distel M, et al. Automated reporter quantification in vivo: high-throughput screening method for reporter-based assays in zebrafish. PLoS One. 2012;7:e29916.
24. Takeuchi M, Matsuda K, Yamaguchi S, Asakawa K, Miyasaka N, Lal P, et al. Establishment of Gal4 transgenic zebrafish lines for analysis of development of cerebellar neural circuitry. Dev Biol. 2015;397:1–17.
25. Westerfield M. The Zebrafish Book. A Guide for the Laboratory Use of Zebrafish (Danio rerio). 4th ed. Eugene: University of Oregon Press; 2000.
26. Licitra R, Fronte B, Verri T, Marchese M, Sangiacomo C, Santorelli FM. Zebrafish feed intake: a systematic review for standardizing feeding management in laboratory conditions. Biology. 2024;13:209.
27. Marchese M, Pappalardo A, Baldacci J, Verri T, Doccini S, Cassandrini D, et al. Dolichol-phosphate mannose synthase depletion in zebrafish leads to dystrophic muscle with hypoglycosylated α-dystroglycan. Biochem Biophys Res Commun. 2016;477:137–43.
28. Livak KJ, Schmittgen TD. Analysis of relative gene expression data using real-time quantitative PCR and the 2(-Delta Delta C(T)) Method. Methods. 2001;25:402–8.
29. Michelucci E, Giorgi ND, Finamore F, Smit JM, Scholte AJHA, Signore G, et al. Lipid biomarkers in statin users with coronary artery disease annotated by coronary computed tomography angiography. Sci Rep. 2021;11:12899.
30. Wiśniewski JR, Zougman A, Nagaraj N, Mann M. Universal sample preparation method for proteome analysis. Nat Methods. 2009;6:359–62.
31. Laakkonen EK, Soliymani R, Karvinen S, Kaprio J, Kujala UM, Baumann M, et al. Estrogenic regulation of skeletal muscle proteome: a study of premenopausal women and postmenopausal MZ cotwins discordant for hormonal therapy. Aging Cell. 2017;16:1276–87.

32. Doccini S, Morani F, Nesti C, Pezzini F, Calza G, Soliymani R, et al. Proteomic and functional analyses in disease models reveal CLN5 protein involvement in mitochondrial dysfunction. Cell Death Discov. 2020;6:18.
33. Krämer A, Green J, Pollard J Jr, Tugendreich S. Causal analysis approaches in ingenuity pathway analysis. Bioinformatics (Oxford, England). 2014;30:523–30.
34. Evans BL, Hurlstone AFL, Clayton PE, Stevens A, Shiels HA. Glucose uptake as an alternative to oxygen uptake for assessing metabolic rate in Danio rerio larvae. Curr Res Physiol. 2022;5:216–23.
35. Masek M, Zang J, Mateos JM, Garbelli M, Ziegler U, Neuhauss SCF, et al. Studying the morphology, composition and function of the photoreceptor primary cilium in zebrafish. Methods Cell Biol. 2023;175:97–128.
36. Cozzolino O, Sicca F, Paoli E, Trovato F, Santorelli FM, Ratto GM, et al. Evolution of epileptiform activity in zebrafish by statistical-based integration of electrophysiology and 2-Photon $Ca^{2+}$ imaging. Cells. 2020;9:769.
37. Simonati A, Williams RE, Nardocci N, Laine M, Battini R, Schulz A, et al. Phenotype and natural history of variant late infantile ceroid-lipofuscinosis 5. Dev Med Child Neurol. 2017;59:815–21.
38. Haltia M. The neuronal ceroid-lipofuscinoses. J Neuropathol Exp Neurol. 2003;62:1–13.
39. Bernardi S, Gemignani F, Marchese M. The involvement of Purkinje cells in progressive myoclonic epilepsy: focus on neuronal ceroid lipofuscinosis. Neurobiol Dis. 2023;185:106258.
40. von Schantz C, Saharinen J, Kopra O, Cooper JD, Gentile M, Hovatta I, et al. Brain gene expression profiles of Cln1 and Cln5 deficient mice unravels common molecular pathways underlying neuronal degeneration in NCL diseases. BMC Genomics. 2008;9:146.
41. Murray SJ, Mitchell NL. Natural history of retinal degeneration in ovine models of CLN5 and CLN6 neuronal ceroid lipofuscinoses. Sci Rep. 2022;12:3670.
42. Heins-Marroquin U, Jung PP, Cordero-Maldonado ML, Crawford AD, Linster CL. Phenotypic assays in yeast and zebrafish reveal drugs that rescue ATP13A2 deficiency. Brain Commun. 2019;1:fcz019.
43. Scifo E, Szwajda A, Dębski J, Uusi-Rauva K, Kesti T, Dadlez M, et al. Drafting the CLN3 protein interactome in SH-SY5Y human neuroblastoma cells: a label-free quantitative proteomics approach. J Proteome Res. 2013;12:2101–15.
44. Huttlin EL, Ting L, Bruckner RJ, Gebreab F, Gygi MP, Szpyt J, et al. The BioPlex Network: A Systematic Exploration of the Human Interactome. Cell. 2015;162:425–40.
45. Huttlin EL, Bruckner RJ, Paulo JA, Cannon JR, Ting L, Baltier K, et al. Architecture of the human interactome defines protein communities and disease networks. Nature. 2017;545:505–9.
46. Parviainen L, Dihanich S, Anderson GW, Wong AM, Brooks HR, Abeti R, et al. Glial cells are functionally impaired in juvenile neuronal ceroid lipofuscinosis and detrimental to neurons. Acta Neuropathol Commun. 2017;5:74.
47. Savchenko E, Singh Y, Konttinen H, Lejavova K, Mediavilla Santos L, Grubman A, et al. Loss of Cln5 causes altered neurogenesis in a mouse model of a childhood neurodegenerative disorder. Dis Model Mech. 2017;10:1089–1100.
48. Schmiedt ML, Blom T, Blom T, Kopra O, Wong A, von, et al. Cln5-deficiency in mice leads to microglial activation, defective myelination and changes in lipid metabolism. Neurobiol Dis. 2012;46:19–29.
49. Fueki N, Iinuma K, Kojima A, Yanai K, Haginoya K, Tada K, et al. Reduced regional cerebral metabolic rate for glucose at the terminal stage in a case of late infantile neuronal ceroid lipofuscinosis. J Child Neurol. 1990;5:98–100.
50. Cooper JD, Messer A, Feng AK, Chua-Couzens J, Mobley WC. Apparent loss and hypertrophy of interneurons in a mouse model of neuronal ceroid lipofuscinosis: evidence for partial response to insulin-like growth factor-1 treatment. J Neurosci. 1999;19:2556–67.
51. Santucci L, Bernardi S, Santorelli FM, Marchese M. Impairment of glucose metabolism as a hallmark of progressive myoclonus epilepsies: focus on the neuronal ceroid lipofuscinoses. Front Cell Neurosci. 2024;18:1445003.
52. Owen MR, Doran E, Halestrap AP. Evidence that metformin exerts its anti-diabetic effects through inhibition of complex 1 of the mitochondrial respiratory chain. Biochem J. 2000;348:607–14.
53. Zhang CS, Li M, Ma T, Zong Y, Cui J, Feng JW, et al. Metformin activates AMPK through the lysosomal pathway. Cell Metab. 2016;24:521–2.
54. Pawlyk AC, Giacomini KM, McKeon C, Shuldiner AR, Florez JC. Metformin pharmacogenomics: current status and future directions. Diabetes. 2014;63:2590–9.
55. Lopez-Fabuel I, Garcia-Macia M, Buondelmonte C, Burmistrova O, Bonora N, Alonso-Batan P, et al. Aberrant upregulation of the glycolytic enzyme PFKFB3 in CLN7 neuronal ceroid lipofuscinosis. Nat Commun. 2022;13:536.
56. Huber RJ. Correction to: Molecular networking in the neuronal ceroid lipofuscinoses: insights from mammalian models and the social amoeba Dictyostelium discoideum. J Biomed Sci. 2020;27:94.
57. Furuya S. An essential role for de novo biosynthesis of L-serine in CNS development. Asia Pac J Clin Nutr. 2008;17: Suppl 1. 312–5.
58. Chen X, Calandrelli R, Girardini J, Yan Z, Tan Z, Xu X, et al. PHGDH expression increases with progression of Alzheimer's disease pathology and symptoms. Cell Metab. 2022;34:651–3.
59. Neame S, Safory H, Radzishevsky I, Touitou A, Marchesani F, Marchetti M, et al. The NMDA receptor activation by d-serine and glycine is controlled by an astrocytic Phgdh-dependent serine shuttle. Proc Natl Acad Sci USA. 2019;116:20736–42.

## ACKNOWLEDGEMENTS

We are grateful to Dr. Baldassare Fronte of the University of Pisa for his technical support in the management of the zebrafish facility. The authors thank the Italian patients' association (A-NCL) for their constant encouragement and support. Proteomics measurements were performed at the Meilahti Clinical Proteomics Core Facility (supported by HiLIFE and Biocenter Finland). Dr. Maria Marchese has received an EMBO Scientific Exchange Grant (number 9681) to conduct research in the lab of Dr. Stephan Neuhauss (Department of Molecular Life Sciences, University of Zurich, Zürich, Switzerland). The topic of the research project was "Discovering new insight on retinal defects in the cln5 zebrafish model using ERG recordings as a tool".

## AUTHOR CONTRIBUTIONS

Conceptualization: M.M.; Methodology: M.M. S.B., R.V.; S.D.; L.S; R.S.; S.M.; R.L; A.O.; L.C. Formal analysis and investigation: M.M.; S.B.; R.V.; S.D.; L.S; M.L.; S.M.; R.L; J.Z; G.S.; L.C. Writing - original draft preparation: M.M.; Writing - review and editing: F.M.S.; S.B.; S.D.; M.L.; S.M.; R.L; J.Z.; S.N.; R.S.; G.S.; Funding acquisition: M.M. and F.M.S. Resources: M.M. and F.M.S.; Supervision: M.M. and F.M.S.

## FUNDING

This work was partially supported by the Italian Ministry of Health (Ricerca Finalizzata SG-2018-12367839 to M.M.; Ricerca Corrente 2024-2025, RC 5 × 1000 to M.M. and F.M.S); the Telethon Foundation (grants GSA23C003 and GGP20011 to M.M.). M.M. is the holder of the Telethon Career Award.

## DATA SHARING STATEMENT

MS data presented in this study can be found in online repositories. The proteomics data were submitted to MassIVE (accession number MSV000095679) and ProteomeXchange (accession number PXD055114).

## COMPETING INTERESTS

The authors declare no competing interests.

## ETHICS

The generation of the mutant, using CRISPR/Cas9 technology, was performed with the ethical approval of the Italian Ministry of Health (approval n° 584/2019-PR), in accordance with the European Union's Directive 2010/63/EU on the protection of animals used for scientific purposes, under the supervision of the University of Pisa Animal Care and Use Committee, and in compliance with the 3R principles.

## ADDITIONAL INFORMATION

**Supplementary information** The online version contains supplementary material available at https://doi.org/10.1038/s41380-025-03043-8.

**Correspondence** and requests for materials should be addressed to Maria Marchese or Filippo M. Santorelli.

**Reprints and permission information** is available at http://www.nature.com/reprints

**Publisher's note** Springer Nature remains neutral with regard to jurisdictional claims in published maps and institutional affiliations.

**Open Access** This article is licensed under a Creative Commons Attribution-NonCommercial-NoDerivatives 4.0 International License, which permits any non-commercial use, sharing, distribution and reproduction in any medium or format, as long as you give appropriate credit to the original author(s) and the source, provide a link to the Creative Commons licence, and indicate if you modified the licensed material. You do not have permission under this licence to share adapted material derived from this article or parts of it. The images or other third party material in this article are included in the article's Creative Commons licence, unless indicated otherwise in a credit line to the material. If material is not included in the article's Creative Commons licence and your intended use is not permitted by statutory regulation or exceeds the permitted use, you will need to obtain permission directly from the copyright holder. To view a copy of this licence, visit http://creativecommons.org/licenses/by-nc-nd/4.0/.

© The Author(s) 2025